

Annihilating the Formation of Silicon Carbide: Molten Salt Electrolysis of Carbon–Silica Composite to Prepare the Carbon–Silicon Hybrid for Lithium-Ion Battery Anode

Xianbo Zhou, Hongwei Xie, Xiao He, Zhuqing Zhao, Qiang Ma, Muya Cai, and Huayi Yin* 

Silicon (Si) and carbon (C) composites hold the promise for replacing the commercial graphite anode, thus increasing the energy density of lithium-ion batteries (LIBs). To mitigate the formation of SiC, this paper reports a molten salt electrolysis approach to prepare C-Si composite by the electrolysis of C-SiO₂ composites. Unlike the conventional way of making a C coating on Si, C-SiO₂ composites were prepared by pyrolyzing the low-cost sucrose and silica. The electrochemical deoxidation of the C-SiO₂ composites not only produces nanostructured Si inside the C matrix but also introduces voids between the C and Si owing to the volume shrinkage from converting SiO₂ to Si. More importantly, the use of Mg ion-containing molten salts precludes the generation of SiC, and the electrolytic Si@C composite anode delivers a capacity of about 1500 mAh g⁻¹ after 100 cycles at a current density of 500 mA g⁻¹. Further, the Si@C||LiNi_{0.6}Co_{0.2}Mn_{0.2}O₂ full cell delivers a high energy density of 608 Wh kg⁻¹. Overall, the molten salt approach provides a one-step electrochemical way to convert oxides@C to metals@C functional materials.

1. Introduction

Lithium-ion batteries (LIBs) are the key to underpinning the electrification of modern transportation and using intermittent renewable energies such as solar and wind.^[1–3] To fulfill the requirements of batteries for electric vehicles and grid energy storage, it is necessary to increase the energy densities of LIBs.^[4,5] The use of high-capacity electrode materials is one of the most effective ways to improve the energy densities of LIBs. Si is an earth-abundant element and of a theoretical gravimetric capacity of 3579 mAh g⁻¹, which is ten-fold of the commercially used graphite anode (372 mAh g⁻¹).^[6] This means that one Si atom can accommodate around four Li⁺ to form Li₁₅Si₄ at a fully

charged state, resulting in a vast volume expansion (~300%) of Si.^[7] During discharge, Li⁺ ions will be extracted out from the Si and subsequently incur a significant volume shrinkage thus causing the collapse of Si framework.^[8] After repeated charge and discharge cycles, pulverization of the Si anode becomes severe along with the continual formation of solid electrolyte interface (SEI) layers, so that the active electrode materials gradually lose contact from current collectors and consequently the capacity of the electrode decays.^[9] Therefore, the central focus of developing the high-capacity Si anode is to minimize the capacity fading caused by the huge volume change.


To increase the life span of the Si anode, various approaches have been employed such as designing nanostructured Si materials,^[10–12] preparing Si-C hybrid materials,^[13–18] using buffering matrixes,^[19,20] and engineering electrolytes and binders.^[21–23] It has been proven that the nanostructured Si can reduce the

mechanical stress caused by the volume expansion, and a carbon layer on Si could remarkably stabilize the SEI layers and avoid the disconnection of the Si from the current collector.^[24,25] The conventional approaches preparing nanostructured Si include physical vapor deposition (PVD),^[26] chemical vapor deposition (CVD),^[27] metallurgical reduction,^[14,28,29] ball-milling,^[30] and chemical etching.^[31] In these methods, Si feedstocks are mostly organic Si compounds and Si halides, which require stringent synthesis conditions resulting in high energy consumption and cost. As we know, Si is the second most abundant element in the earth's crust (26.4% by mass), and silica (SiO₂) is the most common natural Si resource. Thus, direct converting silica to nano-Si is of great interests due to the short process, low energy consumption, low cost, and sustainable raw materials.

In addition to the magnesiothermic reduction of solid SiO₂,^[29] direct electrochemical reduction of solid oxides in molten salts offers a straightforward way to extract metals/alloys because the molten salts possess high ionic conductivity and wide electrochemical windows.^[32–34] Si has been successfully prepared by electrochemical reduction of solid silica or soluble silicate in molten CaCl₂-based molten salts.^[35–39] However, the use of CaCl₂-based molten salts could generate CO₃²⁻ at the graphite anode and then the CO₃²⁻ diffuses to the cathode and is then reduced to C, which decreases the coulombic efficiency of the electrolysis.^[40–43] Jin et al. reported that the use of MgCl₂-based molten salt can solve the parasite reactions caused by CO₃²⁻ in molten CaCl₂-

X. Zhou, Prof. H. Xie, X. He, Z. Zhao, Q. Ma, M. Cai, Prof. H. Yin
Key Laboratory for Ecological Metallurgy of Multimetallurgical Mineral of
Ministry of Education, School of Metallurgy, Northeastern University, 110819,
Shenyang China
E-mail: yinhy@smm.neu.edu.cn

Prof. H. Yin
Key Laboratory of Data Analytics and Optimization for Smart Industry
(Northeastern University), Ministry of Education, 110819, Shenyang China
E-mail: yinhy@smm.neu.edu.cn

 The ORCID identification number(s) for the author(s) of this article can be found under <https://doi.org/10.1002/eem2.12062>.

DOI: 10.1002/eem2.12062

based molten salts.^[44,45] Mai et al.^[46] reported that Si nanowires can be prepared by electrode position in molten NaCl-KCl-MgCl₂-CaSiO₃. Yin et al.^[47] tested the Li storage properties of the electrolytic Si film obtained in molten CaCl₂-nano SiO₂, and the capacity retention of the Si film is only 50% after 40 cycles. Recently, Xiao et al. electrodeposited Si nanowires on a carbon cloth and revealed that the surface oxide layer significantly plagued the performance of the electrolytic Si.^[48] However, there are few studies reporting the use of the electrolytic Si from the electrochemical reduction of solid SiO₂ for the anode in LIBs. Since the properties of the Si are highly related to its structures such as morphologies, particle size, and porosities,^[46,49,50] the electrochemical reduction of solid SiO₂ involves both solid reduction and dissolution mechanism,^[51] so that the morphologies of the electrolytic Si are difficult to control.

Precoating a carbon layer on SiO₂ (SiO₂@C) could be an effective strategy to prepare the Si@void@C because the voids can be created by the volume shrinkage from converting SiO₂ to Si. Unfortunately, the electrolysis of SiO₂@C in molten CaCl₂ generates SiC but not the Si@C.^[47,52–56] Likewise, the magnesiothermic reduction of SiO₂@C generates SiC or Si@SiC but not the Si@C.^[57,58] Xiao et al. designed a Si@C@Si structure by the electrolysis of SiO₂@polydopamine (PDA) in molten CaCl₂-NaCl at 800 °C and revealed that the SiC could be retarded by the generated gas of thermal decomposition of the PDA.^[48] The obtained Si@C@Si delivered a capacity of 904 mAh g⁻¹ at 500 mA g⁻¹ after 100 cycles. Yoo et al.^[59] reported that the interface of C/SiO₂ played a determining role in manipulating the products of the magnesiothermic reduction of the mixture of SiO₂ and C. Therefore, elimination of SiC by engineering the interface of SiO₂/C in the

process of the (electro-) reduction of SiO₂@C is the key to preparing Si@C (Figure 1).

Note that Si@C could be prepared by magnesiothermic reduction of SiO₂@void@C, but the reduction of the SiO₂@C will concomitantly generate SiC.^[59,60] Unlike the magnesiothermic reduction, the electrochemical reduction process could be engineered by alternating the electrochemical potentials and electrolytes. To suppress the formation of SiC by the electrolysis of SiO₂@C, the MgCl₂-based molten salts were applied. In this work, the SiO₂@C was prepared by pyrolyzing the mixture of silica and sucrose. Then, the Si@C was prepared by the electrochemical reduction of SiO₂@C without generation of SiC in the Mg-based molten salts, and the electrochemical performances of the electrolytic C-Si composite were studied as the anode for LIBs.

2. Results and Discussion

2.1. Electrochemical Preparation of C-Si Composite

Figure 2a depicts the procedure of synthesizing the C-Si composite by electrolysis of SiO₂@C. First, a white powder was obtained after the gel solution was dried (denoted as SiO₂@sucrose). After pyrolysis, the white SiO₂@sucrose precursor turned to black (denoted as SiO₂@C). This result agrees well with the results reported by Yu et al.^[61] The electrolytic product (C/Si = 1, molar ratio) obtained at 2.3 V for 13 h in the molten salt was black, and the products turned to slightly yellowish when the C/Si ratio decreased to 0.7 and 0.5 (Figure S1). According to thermogravimetric analysis, the carbon contents of samples with different C/Si ratios (0.5, 0.7, and 1) were 10.7%, 19.2%, and 27.7%, respectively (Figure S2). The measured carbon contents are slightly lower than designed value because some carbon may be lost during the water leaching process. Note that all electrolytic products contained amorphous C and Si without the formation of SiC (Figure 3). Thus, the molten salt plays a key role in preventing the formation of SiC. The electrochemical preparation of Si@C from SiO₂ and sucrose is shown in Figure 2b. During electrolysis, SiO₂ encapsulated in the C matrix is reduced to Si at the cathode. Notably, the theoretical atomic volume of Si is smaller than SiO₂, that is, 1 mol of Si accounts for 52 vol% of 1 mol of SiO₂ precursor. This means that the electrochemical reduction of SiO₂ not only removes O²⁻ but also creates voids that are beneficial to overcome the volume expansion of Si during the lithiation process.

Nano-SiO₂, SiO₂@sucrose, and SiO₂@C are all amorphous, indicating that the pyrolysis does not cause the crystallization of both SiO₂ and C (Figure 3a). After electrolysis, the electrolytic product contains Si and Mg₂SiO₄ at 2.2 V, Si and MgO at 2.3 and 2.4 V (Figure 3b,c). The MgO can be washed away by dissolving in a HCl solution (Figure 3c) and in principle, the obtained MgCl₂ can be reused when scaling up the electrolysis cell. Note that SiC was not formed, which was quite different from the electrochemical reduction of SiO₂@C in molten CaCl₂^[54,56,62] and magnesiothermic reduction of SiO₂@C.^[63] Compared with the magnesiothermic reduction,^[64] the electrochemical reduction occurs without the help of the Mg when the potential of the cathode is more positive than that of Mg deposition. Different from molten CaCl₂ that has a high solubility of CaO,^[65] the Mg-based molten salt has a low solubility of MgO so that the generated MgO stays at the cathode.^[45] As a result, the in situ formed MgO could isolate the electrolytic Si from C thereby suppressing the formation of SiC. Thus, the reactions in molten NaCl-KCl-MgCl₂ are shown as follows:

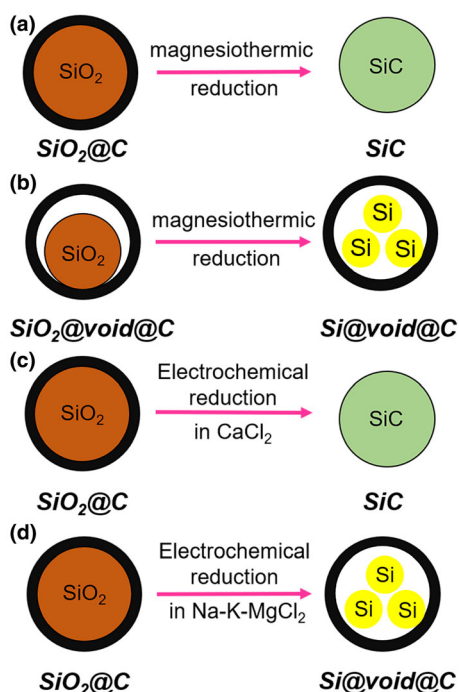
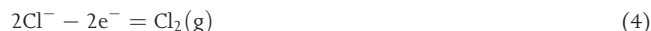


Figure 1. Schematic illustration of manipulating the preparation of Si@C or SiC by magnesiothermic reduction and molten salt electrochemical reduction.

Reactions at the cathode:



The reaction at the anode:



The overall reactions:



During the electrolysis, a current plateau at the beginning of the first 2 h is due to the growth of the current collector/SiO₂/molten salt three-phase interlines (Figure S3), which agrees well with the common behaviors of electroreduction of solid oxides in molten salts.^[66] Note that the reduction of SiO₂ may involve a high potential drop caused by the poor electrical conductivity of Si, especially at a relatively low temperature. As shown in Figure S4, an obvious sandwich structure was observed in the electrolytic product after being electrolyzed for 20.5 h. By using the mixture of SiO₂ and C, the pellets can be fully reduced to Si in 13 h, suggesting that the C considerably decreases the IR drop, thereby accelerating the rate of electrochemical reduction of SiO₂. On the anode side, chlorine gas will be generated and the chlorine gas should be absorbed by an alkaline solution or be used for the chlorination.

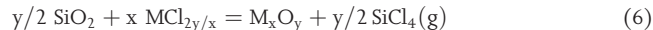
The morphologies of SiO₂, SiO₂@sucrose, and SiO₂@C are uniform (Figure 4a–c). After electrolysis, the electrolytic products show agglomerated nanoparticles (Figure 4d–f), which are very different from the products prepared by the electrolysis of solid SiO₂ in molten CaCl₂.^[38,67–69] In the molten NaCl–KCl–MgCl₂, the low solubilities of both MgO and SiO₂ may preclude the dissolution–deposition mechanism, and the C matrix may constrain the SiO₂ inside, therefore maintaining the original spherical morphologies. No significant difference was observed from the electrolytic products obtained at 13 and 24 h, meaning that a longer electrolysis time did not change the morphologies of Si. The EDS analysis shows that oxygen content is less than 5wt% (Figure S5).

Although the morphology and dimension of the particles before and after electrolysis are almost identical observed from SEM images (Figure 4c–f), the BET test shows that the surface area before and after electrolysis are extremely different. Before electrolysis, the SiO₂@C only has a specific surface area of 57.4 m² g^{−1} while the surface area of Si@C (after electrolysis, 2.4 V–13 h) is up to 191.9 m² g^{−1} (Figure 5a). At the same time, pore volume increases from 0.068 to 0.27 cm³ g^{−1} after the electrolysis and pickling process (Figure 5b). Such a large change can be attributed to a multitude of pores generated by the volume shrinkage from SiO₂ to Si and the removal of MgO. TEM images also confirm this conclusion. As shown in Figure 4g–h, silicon is encapsulated in the carbon matrix and there are some voids between them. The size of Si particles inside the carbon matrix is 10–20 nm, which is smaller than that of SiO₂ precursor (ca. 30 ± 5 nm), and the thickness of the carbon layer is around 10 nm. Since the carbon coating is inert and its dimension does not change during the electrolysis, the volume shrinkage from SiO₂ to Si creates voids and

increases the BET surface area of the electrolytic Si@C composite. The distance of the labeled lattice is measured to be 0.31 nm, corresponding to the Si(111) (Figure 4h). From Figure 4i, the diffraction rings of Si suggest that the electrolytic Si is in the form of a polycrystalline structure.

2.2. Thermodynamic analysis and the electrochemical reduction behaviors of SiO₂

Thermodynamically, the salts making up the electrolyte have to be more stable than SiO₂. The feasibility of electrochemically reducing SiO₂ depends on the decomposition potential of the most stable oxides in molten salt,^[70] and the sequence of the stability of oxides is shown in Figure S6. The preference of the oxide existing in the molten salt from high to low is SiO₂, MgO, Na₂O, and K₂O in the NaCl–KCl–MgCl₂ melt. It means that SiO₂ is stable in the molten salt because SiO₂ cannot react with NaCl, KCl, and MgCl₂ to form SiCl₄ and Na⁺, K⁺, and Mg-oxides. However, Na₂O and K₂O are not stable in the molten salt because they can spontaneously react with MgCl₂ to form MgO, NaCl, and KCl. In other words, Na₂O and K₂O are not thermodynamically stable oxides in the molten NaCl–KCl–MgCl₂. Thus, the electrochemical reduction SiO₂ to Si can happen in the NaCl–KCl–MgCl₂ melt because the thermodynamically preferable MgO has a higher decomposition potential than SiO₂. The most stable oxides in molten salt could be predicted by Equation (6), and the decomposition of the oxides could be obtained from the Ellingham diagram of the oxides.^[71]



where M refers to Na, K, and Mg, and subscripts x and y are numbers of 1 or 2. The Gibbs free energy change of the Equation (7) is expressed as:

$$\Delta G_{\text{eqn}} = (\Delta G_{\text{fM}_x\text{O}_y} - x \Delta G_{\text{fMCl}_{2y/x}}) - y/2(\Delta G_{\text{fSiO}_2} - \Delta G_{\text{fSiCl}_4}) \quad (7)$$

A positive value of ΔG_{eqn} means that the M_xO_y is less stable than SiO₂, and vice versa. This rule could be used to assess the stability of oxides in oxide-containing molten salt.

Thermodynamically, SiO₂ can be electrochemically reduced to Si if the decomposition potential of SiO₂ is lower than that of the most stable oxides in the molten salt. The deposition potential of SiO₂/Si is more positive than that of Mg, meaning that the ternary NaCl–KCl–MgCl₂ molten salt can be used as the electrolyte for electrochemically reducing SiO₂ to Si (Figure 6a). Moreover, the formation of Mg₂Si occurs when the applied potential is more negative than the deposition potential of Si. Sodium and potassium are hard to deposit because the potential gap between Mg and Na/K is ~1.0 V (Figure 6a). Although increasing the cell voltage can increase the reduction rate, Mg–Si alloys and Mg are the unwanted products when the potential of the cathode is polarized more negatively. In addition, the generation of Mg could react with the carbon that will trigger other reactions.^[72]

A three-electrode setup was used to explore the reduction behaviors of SiO₂ in molten NaCl–KCl–MgCl₂. A pair of redox peaks (c1, a1) at ~−1.5 V (vs Ag) correspond to the deposition and stripping of Mg on an empty Mo MCE (Figure 6b, curve 1). As for the Mo MCE filled with

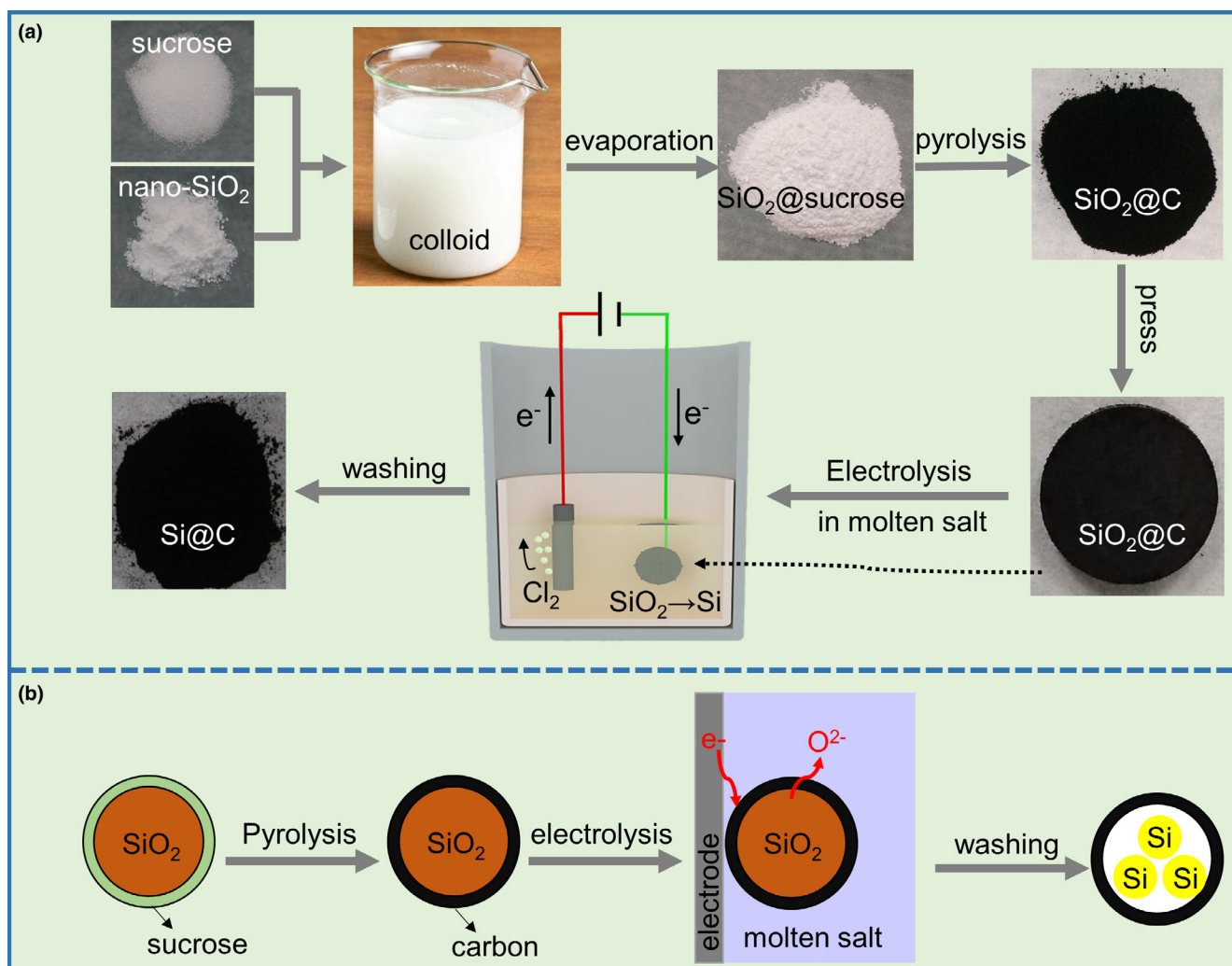


Figure 2. a) Flow sheet and digital pictures of preparing Si@C through a molten salt electrolysis approach in molten NaCl-KCl-MgCl₂. b) Schematic illustration of the formation of Si@C.

SiO₂ (Figure 6b, curve 2), the reduction peak c3 is ascribed to the deoxidation of SiO₂, and the redox peaks (c2, a2) is due to the under-potential deposition and stripping of Mg²⁺ on the electrolytic Si. Under consecutive scans, the reduction peak (c3) significantly decreases in the second cycle while the stripping peak (a2) increases (Figure S7), indicating that the reduction of SiO₂ almost completed in the first cycle and a slight increase of the reduction peak (a2) is due to the increase of electrolytic Si in the second cycle.

2.3. Battery performances

The electrochemical performances of the electrolytic products were evaluated in a half LIB containing a electrolytic Si-C working electrode and a lithium foil as the counter electrode. As shown in Figure 7a, the reduction peak between 1.5 and 0.9 V (vs Li, all potentials are respect to Li unless otherwise specified) may be attributed to the electrochemical reduction of the SiO₂ layer at the surface of Si. A broad reduction peak at 0.76 V (the insert picture in Figure 7a) in the first cycle is due

to the formation of SEI layers.^[60] In the consecutive CV curves, a reduction peak at 0.21 V corresponds to the lithiation reaction of Si to form Li_xSi. Upon the anodic sweep, two peaks at 0.39 and 0.52 V are assigned to the delithiation of Li_xSi.

The electrolytic Si-C has a long flat discharge plateau at 0.11 V in the first cycle (Figure 7b), representing the characteristic plateau of the lithiation of crystalline Si. For evaluating the cycling performance, the Si-C can deliver a specific capacity of 1 800 mAh g⁻¹ in the first 6 cycles (at 0.1 A g⁻¹) while the sucrose-derived carbon only has a capacity of around 200 mAh g⁻¹ (Figure S8). The capacity dropped to 1692 mAh g⁻¹ at 7th cycle and it gradually dropped to 1 496 mAh g⁻¹ at 100th cycle (0.5 A g⁻¹, Figure 7c). Accordingly, the capacity retention rate from the 7th to 100th is 88.4%. Note that the Si@C delivers a high discharge specific capacity of about 1 060 mAh g⁻¹ even at 2 A g⁻¹ (Figure 7d). In contrast, the discharge capacity of pure nano-Si dropped to below 100 mAh g⁻¹ after 40 cycles.^[73] The initial Coulombic efficiencies of the electrolytic Si and Si@C are 60% and 66%, respectively. As for the full battery, the prelithiated electrolytic Si@C can deliver a high reversible capacity of

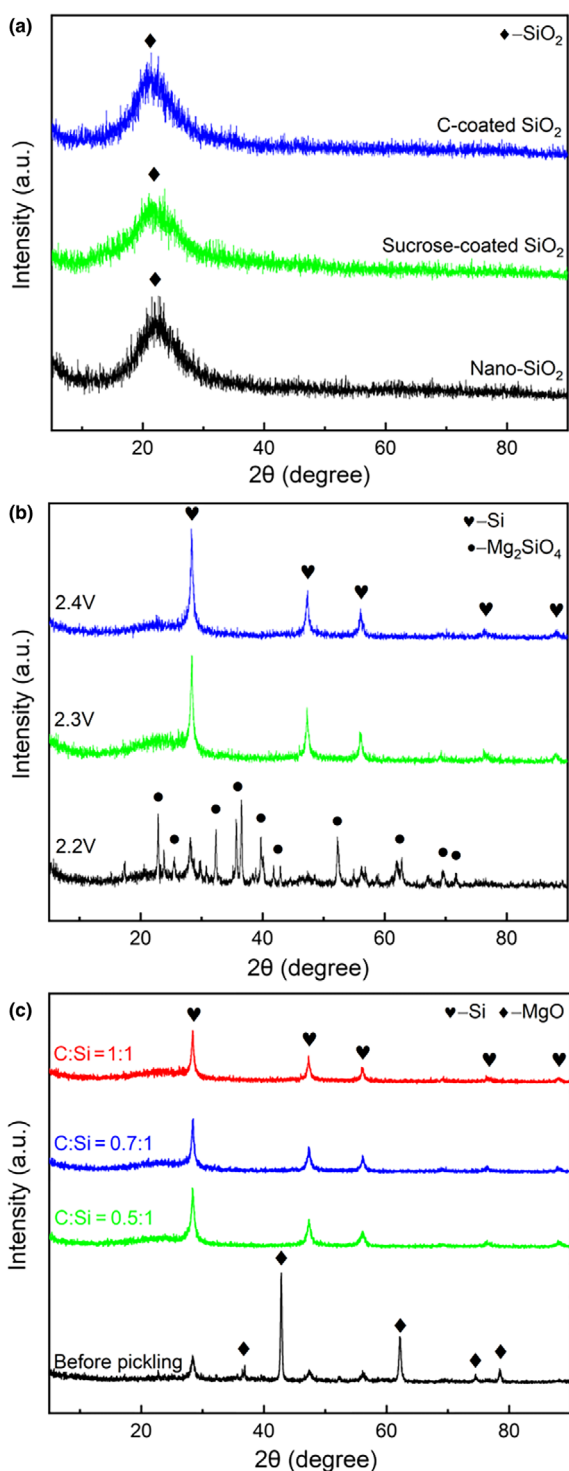


Figure 3. XRD patterns of a) nano-SiO₂, SiO₂@sucrose, and SiO₂@C (C: Si = 1:1), b) electrolytic products obtained at 2.2, 2.3 and 2.4 V for 13 h, respectively (C:Si = 1:1), and c) electrolytic products obtained at 2.3 V for 13 h with a C/Si ratio of 0.5, 0.7, and 1.0 (atomic ratio). All products were prepared in molten NaCl-KCl-MgCl₂ at 650 °C.

~160 mAh g⁻¹ at 0.5C (1C = 160 mAh g⁻¹) with the capacity retention of 80% after 100 cycles. The initial coulombic efficiency was up to 85% (Figure 7e). Taking an average voltage at 3.8 V (Figure 7f), the

full cell can deliver a high energy density of 608 Wh kg⁻¹, which is suitable as the power source for electric vehicles, etc.

To study the effect of C content on the electrolytic products, electrochemical performances of electrolytic products of C/Si ratios of 0.5, 0.7, and 1 were investigated. The C content of electrolytic products was calculated by the sucrose/SiO₂ ratio because the C yield of the sucrose was measured under the same conduction. It is found that the Si@C (2.3 V-13 h) of the C/Si ratio of 1 shows the highest discharge specific capacity of 900 mAh g⁻¹ at 0.5 A g⁻¹ after 100 cycles (Figure 8a). The C content could considerably influence the structure of the electrolytic Si@C, thereby enhancing the buffering effect and reducing diffusion path of Li ions. The discharge capacities of Si-C composites are, respectively, 600 and 400 mAh g⁻¹ after 100 cycles when the C/Si ratios are set at 0.7 and 0.5 (Figure 8a). In addition to cyclability, a lower C content corresponds to a poorer rate capability (Figure S9). The capacity fade rate increases with decreasing C/Si ratio, meaning that increasing C is beneficial to improve both the cyclability and rate capability of the Si@C. In general, a lower C content corresponds to a higher initial discharge capacity. However, the utilization of Si is related to the C content, which should be further researched.

The effect of the electrolysis voltage on the electrochemical performances of the electrolytic Si@C was investigated. Obviously, the electrolytic Si@C obtained 2.4 V-13 h delivers a higher specific capacity of 1 200 mAh g⁻¹ at 0.5 A g⁻¹ after 100 cycles and has a slower fading rate than that obtained at 2.3 V-13 h (Figure 8b). In general, a higher electrolysis voltage corresponds to a higher driving force for removing the oxide ions from the cathode during the electrolysis. To further remove the oxygen inside the electrolytic products, the electrolysis time was extended from 13 to 24 h. It is found that the electrochemical performances of the Si@C are further improved when the electrolysis time is increased from 13 to 24 h (Figure 8c). As shown in Figure 8d, the electrolytic product obtained at 2.4 V-24 h delivers ~1500 mAh g⁻¹ at 0.5 A g⁻¹, ~1 400 mAh g⁻¹ at 1 A g⁻¹, and ~1100 mAh g⁻¹ at 2 A g⁻¹ after 100 cycles. Thus, extending the electrolysis time could improve the electrochemical performances of the Si@C, which could be due to a lower oxygen content of the electrolytic Si. To confirm this assumption, the chemical information of electrolytic Si@C obtained at 2.4 V for 13 and 24 h was detected by XPS. Obviously, the product obtained from a longer electrolysis time possesses a relatively low intensity of Si-O bond, and SiC was not observed (Figure 9a). The mass percentages of different elements calculated based on the XPS spectra are shown in Figure S10. Note that the oxygen contents are 7.5 and 3.9 wt% for the electrolytic samples obtained at 2.3 V for 13 and 24 h, respectively. This means that the oxygen content decreases with increasing the electrolysis time. A higher oxygen content of the electrolytic Si@C could consume more electrolyte to convert SiO₂ to Si and simultaneously produce Li₂O or other Li compounds, thereby decreasing the utilization of the Si and deteriorating the battery performance.

Compared with the bare electrolytic Si, the improved cycling performance of the electrolytic Si-C composite is attributed to the C matrix providing pathways for conducting electrons and lithium ions. On the other hand, the voids incurred by the electrochemical reduction of solid SiO₂ can buffer the huge volume changes of Si during lithiation. Although the theoretical volume of voids caused by electrochemical reduction only accounts for 48% of SiO₂, these voids can somehow release the stress raised by the volume

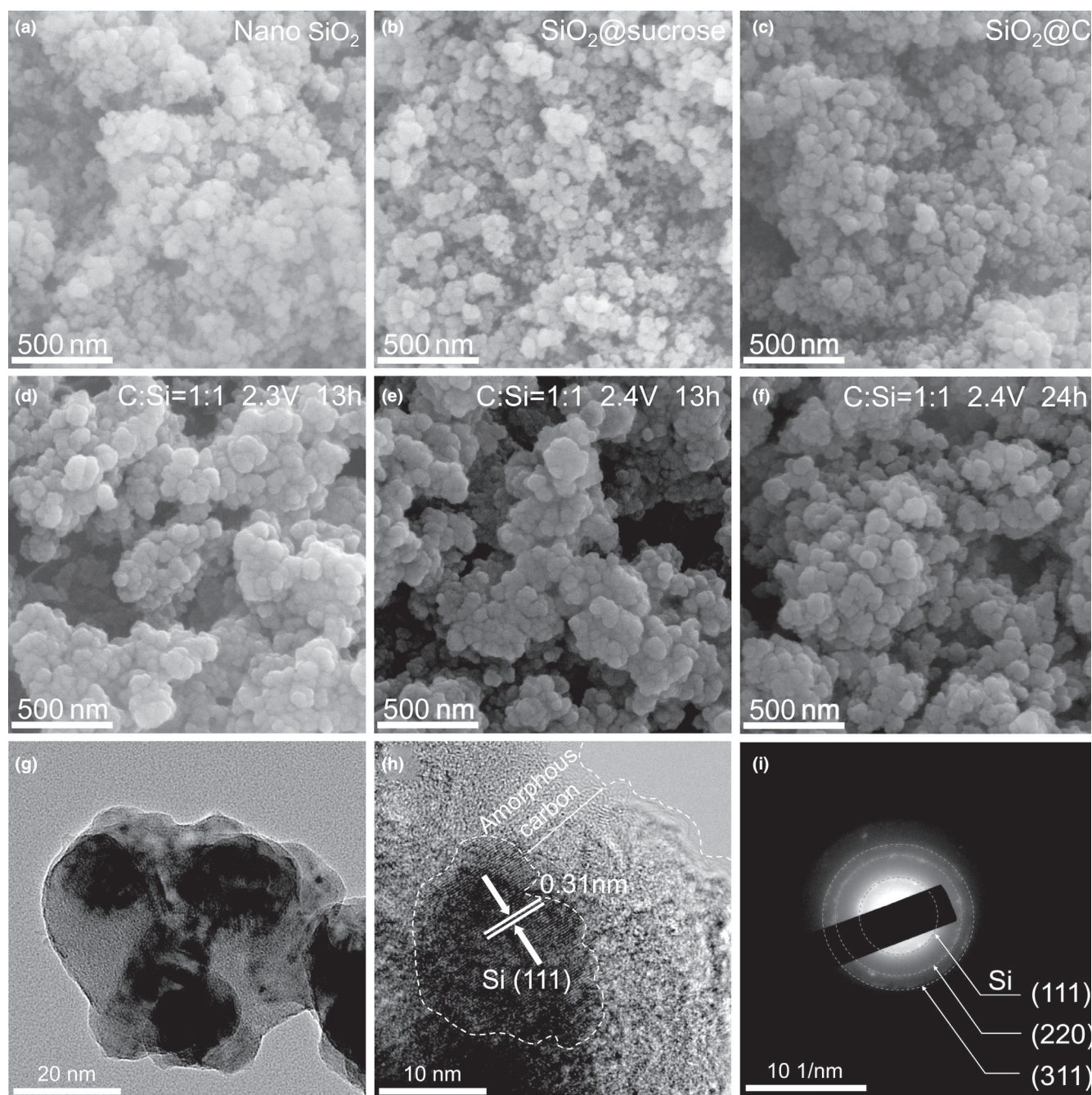


Figure 4. a) SEM images of SiO₂ nanoparticles, b) SiO₂@sucrose, c) SiO₂@C (C/Si = 1), d–f) the electrolytic products obtained at 2.3 V-13 h d) the electrolytic products obtained at 2.3 V-13 h, e) the electrolytic products obtained at 2.4 V-13 h, and f) the electrolytic products obtained at 2.4 V-24 h. g) TEM images of electrolytic product obtained at 2.4 V-24 h. h) The lattice patterns i) Diffraction rings of the electrolytic Si.

expansion of the Si. More importantly, engineering the cell voltage and durations of the electrolysis is helpful to decrease oxygen content so as to improve the performance of the battery. At last, the employment of MgCl₂-based molten salts prevents the formation of SiC, allowing the preparation of Si@C by the direct electrolysis of SiO₂@C in molten salts. In addition, the Li-ion storage performance could be improved by further engineering the electrolysis and configuration of Si and C.

3. Conclusions

Si-C composites have been directly prepared by electrochemical reduction of SiO₂@C in molten NaCl-KCl-MgCl₂ at 650 °C, and the use of Mg-based molten salts can prevent the generation of SiC. After electrolysis, Si was generated in the sucrose-derived C matrix, creating voids by the volume shrinkage from converting SiO₂ to Si. Both C matrix and voids are helpful to tolerate the volume

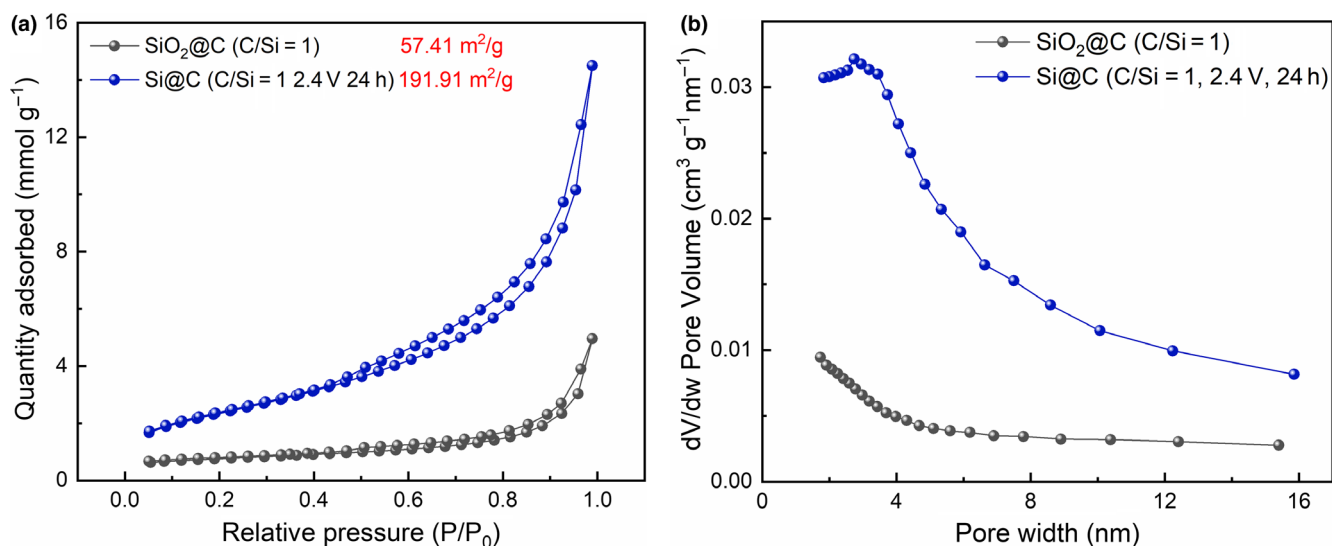


Figure 5. a) Nitrogen adsorption-desorption isotherms of $\text{SiO}_2@\text{C}$ (before electrolysis, $\text{C/Si} = 1$) and $\text{Si}@\text{C}$ (after electrolysis, $\text{C/Si} = 1$, 2.4 V, 13 h). b) Pore size distribution of the material before and after electrolysis.

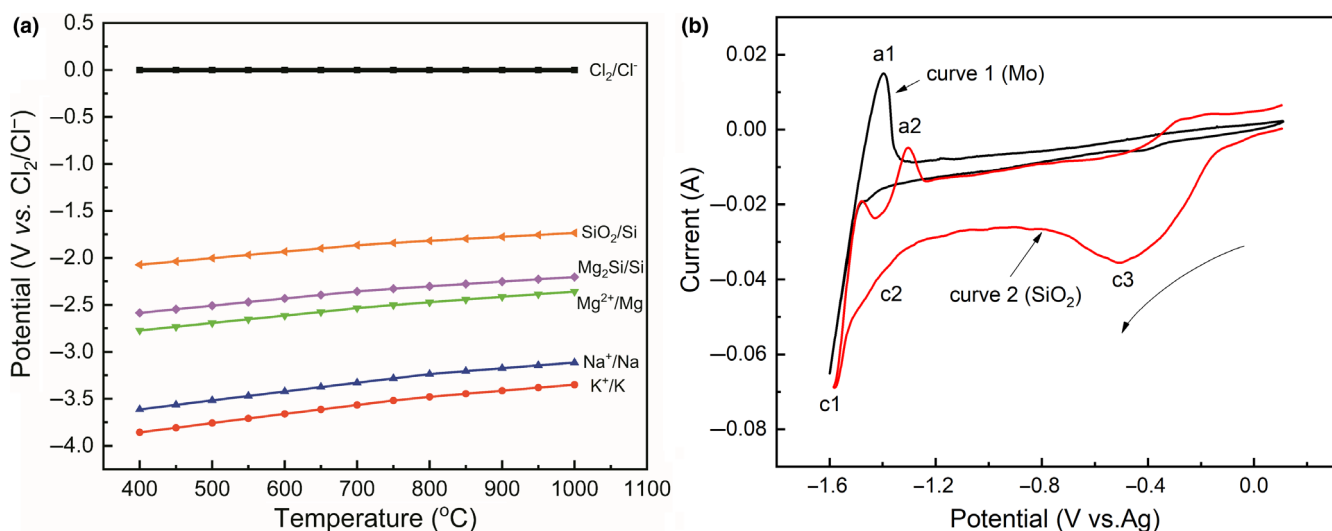


Figure 6. a) Standard potential profiles of various electrochemical reactions as a function of temperature in molten NaCl-KCl-MgCl_2 (all thermodynamic data are from HSC Chemistry 6). b) Cyclic voltammograms (CVs) recorded from the Mo micro-cavity electrode filled with (curve 2) and without (curve 1) SiO_2 in molten NaCl-KCl-MgCl_2 at 650 °C, scan rate: 100 mV s^{-1} .

expansion of Si thereby improving the electrochemical performance of the Si-C composite that delivers a specific capacity of 1500 mAh g^{-1} at 0.5 A g^{-1} and over 1000 mAh g^{-1} at 2 A g^{-1} after 100 cycles. Moreover, the $\text{Si}@\text{C}||\text{LiNi}_{0.6}\text{Co}_{0.2}\text{Mn}_{0.2}\text{O}_2$ full cell delivered a high energy density of 608 Wh kg^{-1} . In the future, the electrochemical performance can be further improved by optimizing construction of C and SiO_2 feedstocks and tuning the cell voltage and durations of the electrolysis to engineer the structure and oxygen content of the electrolytic products. Overall, molten salt electrolysis is a promising pathway to prepare $\text{Si}@\text{C}$ and/or metals@C not only for LIB anode but also for other applications.

4. Experimental Section

Preparation of the $\text{SiO}_2@\text{C}$ composite: The $\text{SiO}_2@\text{C}$ was prepared by pyrolyzing the mixture of SiO_2 (30 ± 5 nm, >99.9%, Aldrich) and sucrose ($\text{C}_{12}\text{H}_{22}\text{O}_{11}$, >99.9%, Macklin). First, the mixture of nano- SiO_2 and sucrose was prepared by a wet chemical approach, by which nano- SiO_2 powders were completely dispersed in a sucrose solution to form a colloid. Then, the colloid was dried at 80 °C to prepare the mixture of sucrose and nano- SiO_2 . Further, the mixed powder was further dried under vacuum at 60 °C for 12 h. A tube furnace was used to conduct the pyrolysis of the mixed powder under Ar atmosphere at 900 °C for 3 h, and the

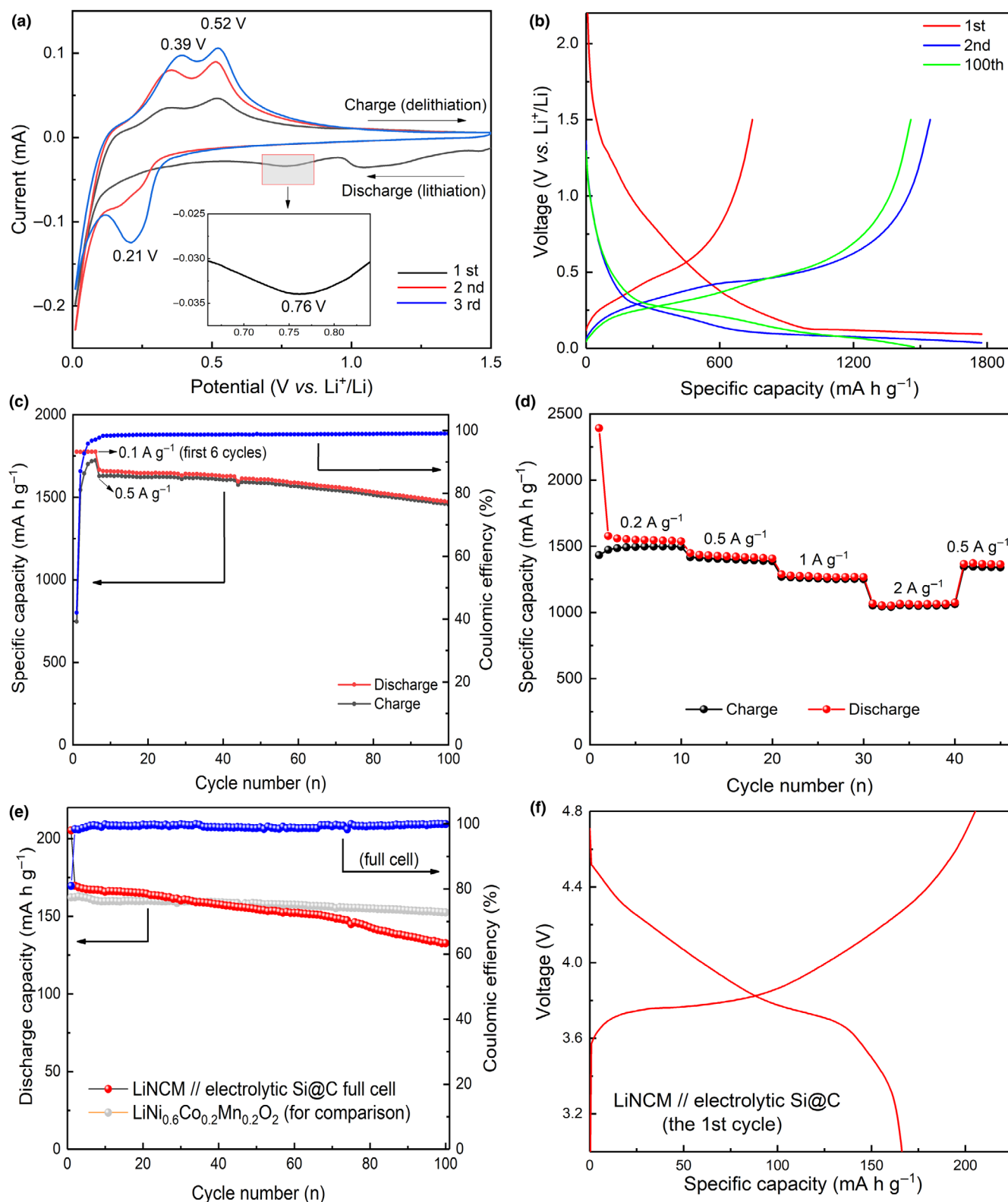


Figure 7. a) CVs of the electrolytic Si@C (C/Si = 1) obtained at 2.4 V for 24 h; b) charge/discharge profiles of the half cell (the maximum charge/discharge specific capacity was set at 1800 mA h g^{-1}); c) cycling performance of the half cell (the maximum charge/discharge specific capacity was set at 1800 mA h g^{-1}); d) rate performance (half-type cell) at various current densities from 0.2 to 2 A g^{-1} ; e) cycling performance of the full cell (the LiNi_{0.6}Co_{0.2}Mn_{0.2}O₂ was used as the cathode in the full cell); and f) first cycle of the charge/discharge profiles of the full cell.

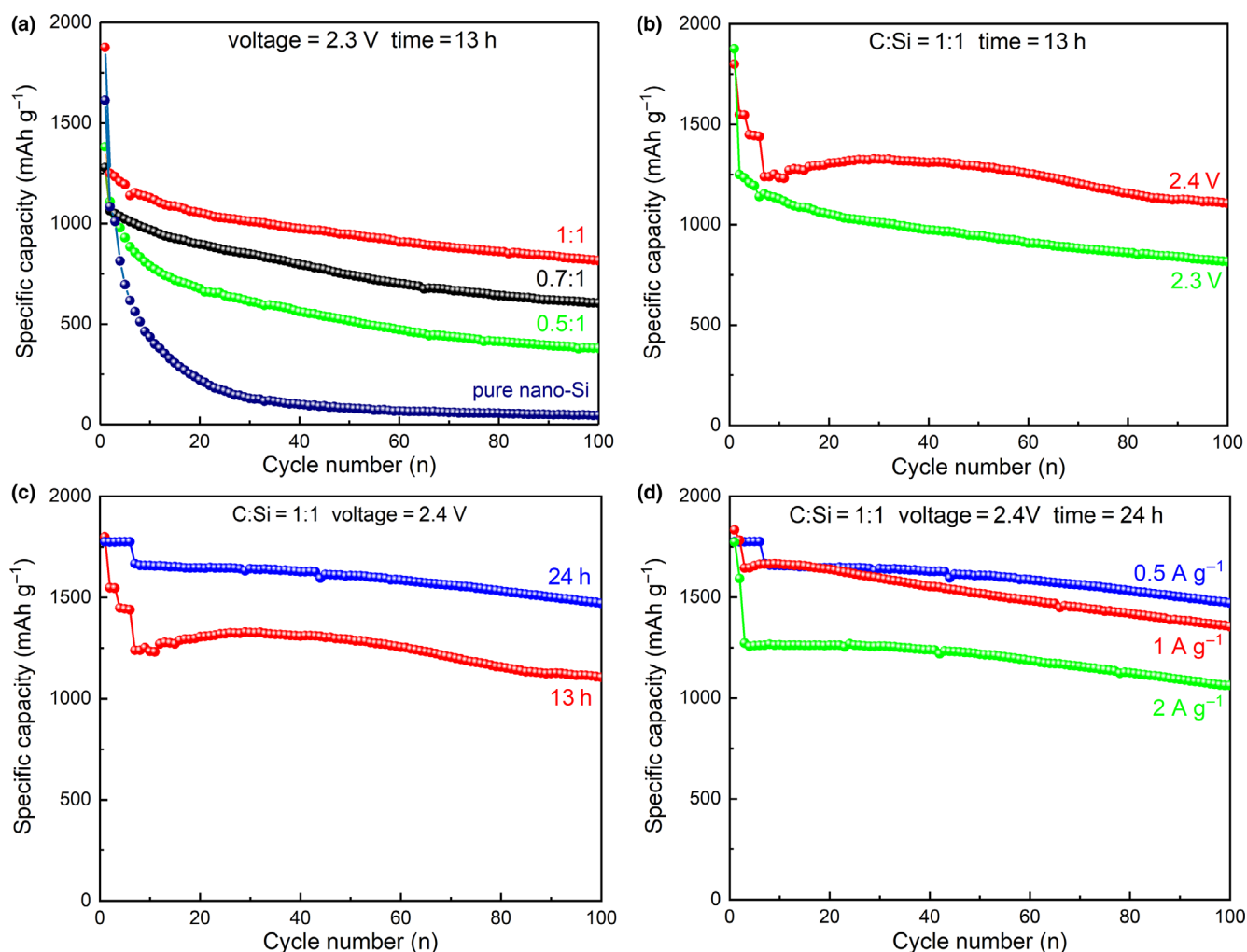


Figure 8. The battery performances of electrolytic products: a) The Si@C of different C/Si ratios (all products were obtained at 2.3 V-13 h), and the discharge rate is 0.5 A g⁻¹; b) the Si@C obtained at 2.3 V-13 h and 2.4 V-13 h, and the discharge rate is 0.5 A g⁻¹; c) the Si@C obtained at 2.4 V-13 h and 2.4 V-24 h, and the discharge rate is 0.5 A g⁻¹; and d) rate capabilities of the Si@C obtained at 2.4 V-24 h. All products were prepared in molten NaCl-KCl-MgCl₂ at 650 °C.

heating rate is 5 °C min⁻¹. After pyrolysis, the furnace was naturally cooled to the room temperature. Note that the carbon yield is 18.7%, which was measured by the pyrolysis of 10 g sucrose with the same procedure for the pyrolysis of the mixture of sucrose and SiO₂. The molar ratios of C/silica were set at 1:1, 0.7:1, and 0.5:1 by controlling the ratio of sucrose/SiO₂ (supposing the C yields of all samples were the same as the pure sucrose).

Electrochemical Reduction Behaviors and Electrolysis of SiO₂@C in Molten Salts: A three-electrode setup was used to conduct the cyclic voltammetry (CV). First, anhydrous NaCl, KCl, and MgCl₂ powders (Na:K:Mg = 0.271:0.221:0.508, molar ratio, >99.5%, Macklin) were mixed in a plastic box by shaking, and the mixture was dried under vacuum in an oven at 300 °C for 12 h. The pre-dried salts (500 g) were put into an alumina crucible (inner diameter: 83 mm and height: 82 mm), and the alumina crucible was sealed in a stainless steel (SS) test vessel heated by a vertical tube furnace. Then, the temperature of the furnace was ramped to 650 °C to melt the salts under Ar flow. Before CV measurements, a pre-electrolysis was conducted between a

graphite anode (diameter: 10 mm, >99.9%) and a nickel sheet cathode (15 × 15 mm²) under a constant cell voltage of 2.2 V for 2 h to further remove the impurities in the molten salt. A molybdenum (Mo) micro-cavity electrode (MCE) filled with SiO₂ powder was used as the working electrode, a silver wire (diameter: 0.5 mm, >99.99%) was used as the quasi-reference electrode, and a graphite rod (diameter: 10 mm, >99.9%) was used as the counter electrode. CV measurements were performed by an electrochemical workstation (CHI 1140, Shanghai Chenhua, Co., Ltd.).

In the same molten salt bath, a two-electrode system was applied to conduct the electrolysis between a graphite anode and a pellet cathode that was made from the as-prepared mixture of silica and C (weight: 1.0 g, diameter: 16 mm, and thickness: 4 mm) under a pressure of ~4 MPa. The tablets were sintered at 750 °C (ramping rate is 5 °C min⁻¹) for 3 h to increase their mechanical strength. After electrolysis, the cathode was taken out of the molten salt and cooled down in the upper space of the test vessel, further removed from the test vessel, washed with a hydrochloric acid solution (1 mol L⁻¹, 50 °C) and deionized water to remove the salts and MgO within the electrolytic

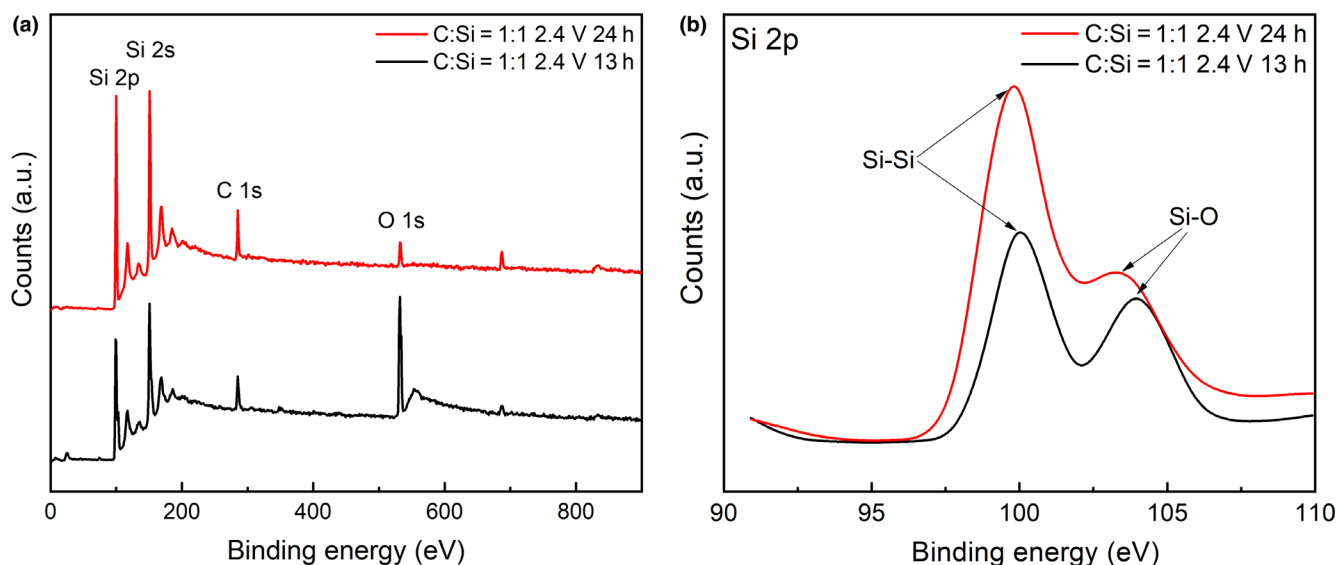


Figure 9. XPS analysis of electrolytic Si@C at a) 2.4 V for 13 h and b) 24 h (C/Si = 1).

product, and finally, it was dried under vacuum (80 °C, 12 h) for further characterization.

Electrochemical Performances of the Electrolytic Si@C: The electrochemical performances of the electrolytic Si@C composite were evaluated using coin cells that were assembled in an argon-filled glove box. The electrolytic Si@C composite was first mixed with super P, sodium alginate in a weight ratio of 6:2:2 (active material:super P:binder), and the mixture was blended with deionized water to form a homogeneous slurry. The slurry was cast onto a copper foil (11 μm in thickness) and vacuum-dried at 50 °C for 12 h. Further, circular disk (12 mm in diameter, 1.13 cm^2 in area) electrodes were prepared by a punching machine. The mass loading of each circular electrode was about 1 mg cm^{-2} for all samples. The electrolyte was 1 mol L^{-1} lithium hexafluorophosphate (LiPF_6) dissolved in a mixed solvent of ethylene carbonate (EC) and diethyl carbonate (DEC) (1:1 in volume) containing 5 vol% fluoroethylene carbonate (FEC) as the additive.

The electrochemical performances of the assembled half-cell were measured by CV (CHI 760e, Shanghai Chenhua Co., Ltd.) and galvanostatic charge and discharge tests (Land CT2001A, Wuhan Jinnuo Electronic Co., Ltd.). CV measurements were performed in the potential range from the open-circuit potential (OCP) to 0 V (vs Li/Li^+) at a scan rate of 0.1 mV s^{-1} . The voltage ranges from 0.01 to 1.5 V during the cycling tests.

The full battery was assembled with commercial $\text{LiNi}_{0.6}\text{Co}_{0.2}\text{Mn}_{0.2}\text{O}_2$ (NCM622) cathode and prelithiated electrolytic Si@C anode. The prelithiation procedure was conducted by using the half cell which was mentioned above. It was first lithiated to 0.01 V at 100 mA g^{-1} by galvanostatic discharging and then disassembled in glove box. The Si@C electrode was taken out and coupled with $\text{LiNi}_{0.6}\text{Co}_{0.2}\text{Mn}_{0.2}\text{O}_2$ to make up the full cell. The n/p ratio of the full-cell Si@C||NCM622 is about 1:3 in mass. The voltage ranges from 3.0 to 4.8 V and the current density is 0.5 C (1C = 160 mA g^{-1}) during the following cycling tests. All specific capacities are calculated based on the mass of the active material.

Material Characterization: The crystal structures of all samples before and after molten salt electrolysis were characterized by X-ray diffraction

(XRD, Shimadzu X-ray 6000 with Cu $\text{K}\alpha$ radiation at $\lambda = 1.5406 \text{ \AA}$). The morphologies of all samples were characterized by scanning electron microscopy (SEM, FEI Sirion field emission), energy dispersive spectroscopy (EDS, XFlash-Detector 5010, Bruker), transmission electron microscopy (TEM, Tecnai G220 TWIN microscope operated at 200 kV), and X-ray photoelectron spectroscopy (XPS, Kratos Analytical Ltd.).

Acknowledgements

We greatly thank the financial support from the National Training Program of Innovation and Entrepreneurship for Undergraduates (201810145075), Fundamental Research Funds for the Central Universities (N172505002), NSFC (51704060), and National Thousand Youth Talent Program of China, and the 111 Project (B16009).

Supporting Information

Supporting Information is available from the Wiley Online Library or from the author.

Keywords

anode material, carbon, lithium-ion batteries, molten salt electrolysis, silicon

Received: September 10, 2019

Revised: December 4, 2019

Published online: December 15, 2019

- [1] J. W. Choi, D. Aurbach, *Nat. Rev. Mater.* **2016**, 1, 16013.
- [2] S. Chu, Y. Cui, N. Liu, *Nat. Mater.* **2016**, 16, 16.
- [3] N. Nitta, F. Wu, J. T. Lee, G. Yushin, *Mater. Today* **2015**, 18, 252.
- [4] B. Dunn, H. Kamath, J.-M. Tarascon, *Science* **2011**, 334, 928.

- [5] Y. Jiang, Y. Zhang, X. Yan, M. Tian, W. Xiao, H. Tang, *Chem. Eng. J.* **2017**, 330, 1052.
- [6] X. Su, Q. Wu, J. Li, X. Xiao, A. Lott, W. Lu, B. W. Sheldon, J. Wu, *Adv. Energy Mater.* **2014**, 4, 1300882.
- [7] J. Wang, X. Meng, X. Fan, W. Zhang, H. Zhang, C. Wang, *ACS Nano* **2015**, 9, 6576.
- [8] H. Wu, Y. Cui, *Nano Today* **2012**, 7, 414.
- [9] M. Ashuri, Q. He, L. L. Shaw, *Nanoscale* **2016**, 8, 74.
- [10] H. Kim, M. Seo, M.-H. Park, J. Cho, *Angew. Chem. Int. Edit.* **2010**, 49, 2146.
- [11] N. Liu, H. Wu, M. T. McDowell, Y. Yao, C. Wang, Y. Cui, *Nano Lett.* **2012**, 12, 3315.
- [12] N. Liu, Z. Lu, J. Zhao, M. T. McDowell, H.-W. Lee, W. Zhao, Y. Cui, *Nat. Nanotechnol.* **2014**, 9, 187.
- [13] M. Ko, S. Chae, J. Ma, N. Kim, H. W. Lee, Y. Cui, J. Cho, *Nat. Energy* **2016**, 1, 8.
- [14] Y.-C. Zhang, Y. You, S. Xin, Y.-X. Yin, J. Zhang, P. Wang, X.-S. Zheng, F.-F. Cao, Y.-G. Guo, *Nano Energy* **2016**, 25, 120.
- [15] X. Zhang, L. Huang, P. Zeng, L. Wu, Q. Shen, Z. Gao, Y. Chen, *Chem. Eng. J.* **2019**, 357, 625.
- [16] M. L. Terranova, S. Orlanducci, E. Tamburri, V. Guglielmotti, M. Rossi, *J. Power Sources* **2014**, 246, 167.
- [17] F. Qu, G. She, J. Wang, X. Qi, S. Li, S. Zhang, L. Mu, W. Shi, *J. Phys. Chem. Solids* **2019**, 124, 312.
- [18] T. Mu, P. Zuo, S. Lou, Q. Pan, Q. Li, C. Du, Y. Gao, X. Cheng, Y. Ma, G. Yin, *Chem. Eng. J.* **2018**, 341, 37.
- [19] M. Su, H. Wan, Y. Liu, W. Xiao, A. Dou, Z. Wang, H. Guo, *Powder Technol.* **2018**, 323, 294.
- [20] H. Wu, G. Yu, L. Pan, N. Liu, M. T. McDowell, Z. Bao, Y. Cui, *Nat. Commun.* **2013**, 4, 1943.
- [21] N.-S. Choi, K. H. Yew, K. Y. Lee, M. Sung, H. Kim, S.-S. Kim, *J. Power Sources* **2006**, 161, 1254.
- [22] I. Kovalenko, B. Zdyrko, A. Magasinski, B. Hertzberg, Z. Milicev, R. Burtovyi, I. Lutzenov, G. Yushin, *Science* **2011**, 334, 75.
- [23] L. Zhang, L. Zhang, L. Chai, P. Xue, W. Hao, H. Zheng, *J. Mater. Chem. A* **2014**, 2, 19036.
- [24] A. Magasinski, P. Dixon, B. Hertzberg, A. Kvit, J. Ayala, G. Yushin, *Nat. Mater.* **2010**, 9, 353.
- [25] Z.-L. Xu, X. Liu, Y. Luo, L. Zhou, J.-K. Kim, *Prog. Mater. Sci.* **2017**, 90, 1.
- [26] D. B. Polat, O. Keles, K. Amine, *J. Power Sources* **2014**, 270, 238.
- [27] T. Ma, H. Xu, X. Yu, H. Li, W. Zhang, X. Cheng, W. Zhu, X. Qiu, *ACS Nano* **2019**, 13, 2274.
- [28] Z. Favors, W. Wang, H. H. Bay, Z. Mutlu, K. Ahmed, C. Liu, M. Ozkan, C. S. Ozkan, *Sci. Rep.* **2014**, 4, 5623.
- [29] J. Entwistle, A. Rennie, S. Patwardhan, *J. Mater. Chem. A* **2018**, 6, 18344.
- [30] W. R. Liu, Z. Z. Guo, W. S. Young, D. T. Shieh, H. C. Wu, M. H. Yang, N. L. Wu, *J. Power Sources* **2005**, 140, 139.
- [31] H. Han, Z. P. Huang, W. Lee, *Nano Today* **2014**, 9, 271.
- [32] A. M. Abdelkader, K. T. Kilby, A. Cox, D. J. Fray, *Chem. Rev.* **2013**, 113, 2863.
- [33] W. Xiao, D. Wang, *Chem. Soc. Rev.* **2014**, 43, 3215.
- [34] G. Z. Chen, D. J. Fray, T. W. Farthing, *Nature* **2000**, 407, 361.
- [35] T. Nohira, K. Yasuda, Y. Ito, *Nat. Mater.* **2003**, 2, 397.
- [36] X. B. Jin, P. Gao, D. H. Wang, X. H. Hu, G. Z. Chen, *Angew. Chem. Int. Edit.* **2004**, 43, 733.
- [37] X. Yang, L. Ji, X. Zou, T. Lim, J. Zhao, E. T. Yu, A. J. Bard, *Angew. Chem. Int. Edit.* **2017**, 56, 15078.
- [38] J. Y. Yang, S. G. Lu, S. R. Kan, X. J. Zhang, J. Du, *Chem. Commun.* **2009**, 3273.
- [39] J. Peng, H. Yin, J. Zhao, X. Yang, A. J. Bard, D. R. Sadoway, *Adv. Funct. Mater.* **2018**, 28, 1703551.
- [40] D. Fray, *Faraday Discuss.* **2016**, 190, 11.
- [41] H. W. Xie, H. J. Zhao, Q. S. Song, Z. Q. Ning, J. K. Qu, H. Y. Yin, *J. Electrochem. Soc.* **2018**, 165, E759.
- [42] H. Y. Yin, X. H. Mao, D. Y. Tang, W. Xiao, L. R. Xing, H. Zhu, D. H. Wang, D. R. Sadoway, *Energy Environ. Sci.* **2013**, 6, 1538.
- [43] L. Hu, Y. Song, J. Ge, J. Zhu, Z. Han, S. Jiao, *J. Mater. Chem. A* **2017**, 5, 6219.
- [44] W. Li, Y. Yuan, X. Jin, H. Chen, G. Z. Chen, *Prog. Nat. Sci. Mater. Int.* **2015**, 25, 650.
- [45] Y. T. Yuan, W. Li, H. L. Chen, Z. Y. Wang, X. B. Jin, G. Z. Chen, *Faraday Discuss.* **2016**, 190, 85.
- [46] Y. F. Dong, T. Slade, M. J. Stolt, L. S. Li, S. N. Girard, L. Q. Mai, S. Jin, *Angew. Chem. Int. Edit.* **2017**, 56, 14453.
- [47] H. Xie, H. Zhao, J. Liao, H. Yin, A. J. Bard, *Electrochim. Acta* **2018**, 269, 610.
- [48] W. Weng, W. Xiao, A. C. S. Appl, *Energy Mater.* **2019**, 2, 804.
- [49] J. Zhao, S. M. Lu, L. Y. Hu, C. Li, *J. Energy Chem.* **2013**, 22, 819.
- [50] J. Zhao, H. Y. Yin, T. H. Lim, H. W. Xie, H. Y. Hsu, F. Forouzan, A. J. Bard, *J. Electrochem. Soc.* **2016**, 163, D506.
- [51] W. Xiao, X. Wang, H. Y. Yin, H. Zhu, X. H. Mao, D. H. Wang, *RSC Adv.* **2012**, 2, 7588.
- [52] Y. Liu, K. Hanai, J. Yang, N. Imanishi, A. Hirano, Y. Takeda, *Electrochem. Solid State Lett.* **2004**, 7, A369.
- [53] C. Zhao, J. Yang, S. Lu, *Chin. J. Inorg. Chem.* **2013**, 29, 2543.
- [54] X. Zou, L. Ji, X. Lu, Z. Zhou, *Sci. Rep.* **2017**, 7, 9978.
- [55] D. S. M. Vishnu, J. Sure, H.-K. Kim, J.-Y. Kim, R. V. Kumar, C. Schwandt, *J. Electrochem. Soc.* **2018**, 165, D731.
- [56] H. J. Zhao, H. W. Xie, X. B. Zhou, J. K. Qu, Z. Q. Zhao, Q. S. Song, Z. Q. Ning, P. F. Xing, H. Y. Yin, *J. Electrochem. Soc.* **2019**, 166, E137.
- [57] D. T. Ngo, H. T. T. Le, X.-M. Pham, C.-N. Park, C.-J. Park, A. C. S. Appl, *Mater. Interfaces* **2017**, 9, 32790.
- [58] J. Su, B. Gao, Z. Chen, J. Fu, W. An, X. Peng, X. Zhang, L. Wang, K. Huo, P. K. Chu, *ACS Sustain. Chem. Eng.* **2016**, 4, 6600.
- [59] J. Ahn, H. S. Kim, J. Pyo, J.-K. Lee, W. C. Yoo, *Chem. Mater.* **2016**, 28, 1526.
- [60] S. Chen, L. Shen, P. A. van Aken, J. Maier, Y. Yu, *Adv. Mater.* **2017**, 29, 1605650.
- [61] Y. Yao, J. Zhang, L. Xue, T. Huang, A. Yu, *J. Power Sources* **2011**, 196, 10240.
- [62] D. S. M. Vishnu, J. Sure, H. K. Kim, J. Y. Kim, C. J. J. o. T. E. S. Schwandt, *J. Electrochem. Soc.* **2018**, 165, D731.
- [63] X.-F. Zhang, Z. Chen, Y. Feng, J. Qiu, J. Yao, *ACS Sustain. Chem. Eng.* **2018**, 6, 1068.
- [64] P. Wu, H. Wang, Y. W. Tang, Y. M. Zhou, T. H. Lu, *ACS Appl. Mater. Interfaces* **2014**, 6, 3546.
- [65] S. Wang, F. Zhang, X. Liu, L. Zhang, *Thermochim. Acta* **2008**, 470, 105.
- [66] W. Xiao, X. B. Jin, Y. Deng, D. H. Wang, G. Z. Chen, *Chem. Eur. J.* **2007**, 13, 604–612.
- [67] W. Weng, C. Zeng, W. Xiao, A. C. S. Appl, *Mater. Interfaces* **2019**, 11, 9156.
- [68] J. Y. Yang, S. G. Lu, S. R. Kan, X. J. Zhang, H. Y. Ding, *Chin. J. Inorg. Chem.* **2009**, 25, 756.
- [69] J. Zhao, J. Li, P. Ying, W. Zhang, L. Meng, C. Li, *Chem. Commun.* **2013**, 49, 4477.
- [70] Z. Haijia, X. Hongwei, Z. Xianbo, Q. Jiakang, Z. Zhuqing, S. Qiushi, N. Zhiqiang, X. Pengfei, Y. Huayi, *J. Electrochem. Soc.* **2019**, 166, E137.
- [71] A. Vignes, *Extractive Metallurgy 1*, John Wiley & Sons, Inc., London **2011**.
- [72] Z. Q. Zhao, H. W. Xie, J. K. Qu, H. J. Zhao, Q. Ma, P. F. Xing, Q. S. Song, D. H. Wang, H. Y. Yin, *Batter. Supercaps* **2019**, 2, 1.
- [73] X. Y. Zhou, J. J. Tang, J. Yang, J. Xie, L. L. Ma, *Electrochim. Acta* **2013**, 87, 663.